Journal of Thermal Analysis and Calorimetry (2019) 136:1467–1480
https://doi.org/10.1007/s10973-018-7773-y

The mixed ligand complexes of Co(II), Ni(II), Cu(II) and Zn(II) with coumarilic acid/1,10-phenanthroline

Synthesis, crystal characterization and biological applications

Özge Dağlı[1] · Dursun Ali Köse[1] · Okan İçten[2] · Gülçin Alp Avcı[3] · Onur Şahin[4]

Received: 17 March 2018 / Accepted: 28 September 2018 / Published online: 15 October 2018

Abstract
The coumarilate ($coum^-$) and 1,10-phenanthroline (phen) mixed ligand complexes of Co(II) (**1**), Ni(II) (**2**) Cu(II) (**3**) and Zn(II) (**4**) were synthesized and structural characterizations were performed by using elemental analysis, magnetic susceptibility, solid-state UV–Vis, FTIR spectra, thermoanalytical TG-DTG/DTA and single-crystal X-ray diffraction methods. The Co(II) and Ni(II) complexes are salt-type compounds, and they have two moles phen ligands bound as bidentate, two moles aqua ligands in coordination sphere and two moles anionic $coum^-$ ligand outside of the coordination unit as the counter-ion of the molecular structure. At the same time, the Co(II) and Ni(II) complexes have five moles of aqua ligands as hydrated water outside of the molecules. It was obtained that Cu(II) and Zn(II) complex structures contain one mole of phen ligand, two moles coordinated ($coum^-$) ligand and a one-mole aqua ligand, and the molecules (Cu(II) and Zn(II)) have fivefold structure and obey square pyramidal geometry. Thermal decomposition of each complex started with dehydration (the first removal is the dehydration of complex Co(II) and Ni(II) as removal of hydrate–aqua molecules), and then, the decomposition of organic parts was observed. The thermal dehydration of the complexes takes place in one (Cu(II) and Zn(II)) or two (Co(II) and Co(II)) steps. The decomposition mechanism, thermal decomposition steps and thermal stability of the investigated complexes provide useful data for the interpretation of their structures. The final decomposition products were found to be metal oxides. Some biological applications (antifungal/antibacterial) were performed using structurally characterized compounds.

Keywords Mixed ligand complexes · Biological application · Coumarilate · 1,10-Phenanthroline · Crystal structure · Thermal properties

Introduction

Oxygen-containing heterocyclic compounds are well known to exhibit important biological properties such as antiarrhythmic, spasmolytic, antiviral, anticancer, antifungal and anti-inflammatory activity [1–7]. Today, many of the natural or synthetic derivatives with high oxygen content have pharmaceutical applications [8, 9]. Benzofuran rings and their derivatives from these compounds are also found in our lives in various fields [10]. Coumarilic acid is one of these derivatives and formed from by linking of the 2-furan carboxylic acid ring with the benzene ring (Scheme 1a).

Its general name is benzofuran-2-carboxylic acid also called as coumarilic acid. The theoretical formula of the compound is $C_9H_6O_3$ with a molecular weight of

✉ Dursun Ali Köse
dalikose@hitit.edu.tr

[1] Department of Chemistry, Hitit University, 19030 Çorum, Turkey

[2] Department of Chemistry, Hacettepe University, Beytepe Campus, 06800 Ankara, Turkey

[3] Department of Molecular Biology and Genetics, Hitit University, Ulukavak, Corum, Turkey

[4] Scientific and Technological Research Application Centre, Sinop University, 57000 Sinop, Turkey

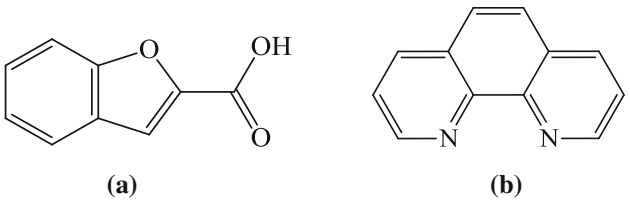

(a) (b)

Scheme 1 The structure of **a** coumarilic acid, **b** 1,10-phenanthroline molecules

162.14 g/mol, and its melting point ranges from 193 to 196 °C. Coumarilic acid is a derivative of coumarin and found in different food sources: fruits, herbs and vegetables [11]. The benzo[b] furan system, as an important pharmacophore, can be found in many compounds and isolated from natural sources. It is also used as a basic part of recently synthesized medicines (such as amiodarone and bergapten) [12, 13].

Although there are many literature data about coumarilic acid complexes of various metal cations, studies on a mixed ligand of coumarilic acid and metal cations are very limited [14, 15]. In the course of the studies, mixed ligand complexes containing single-liganded coumarilic acid and coumarilic acid–nicotinamide ligands were synthesized and examined. The presence of a wide range of physiological and biological effects of coumarilic acid and the ligands used is important for both medical and inorganic chemistry and increases the importance of this study.

1,10-Phenanthroline selected as the neutral ligand of counter-ligand complexes, as shown in Scheme 1b, is the name used to denote heterocyclic ring systems. These heterocyclic rings are formed by the replacement of –CH groups in the phenanthrene ring system by –N=groups. These ring systems are termed as 4,5-diazaphenanthrene, 1,5-diazaphenanthrene and 1,8-diazaphenanthrene.

1,10-Phenanthroline has a planar heterophasic structure and forms stable complexes with transition metals. These stable complexes are widely used in the design of many electronic devices such as field-effect transistors, light-emitting diodes (LED), lasers and photovoltaic batteries [16–18]. 1,10-Phenanthroline–copper(II) complexes and their derivatives are of great interest because of their many biological effects such as inhibition of microbicidal activity, cancer and tumor formation [19].

In this study, it was aimed to synthesize mixed ligand coordination compounds containing ligands of coumarilic acid–1,10-phenanthroline of Co(II), Ni(II), Cu(II) and Zn(II) transition metals. The structures of these synthesized complexes were characterized by elemental analysis, Fourier transforms infrared spectroscopy (FTIR), thermogravimetric analysis (TGA/DTA), single-crystal X-ray diffraction diffractometry (SC-XRD), solid-state ultraviolet–visible region spectroscopy (UV–Vis), magnetic susceptibility and melting point determination methods. Further biological experiments were applied to the complexes.

Experimental

Materials and methods

The chemicals $Co(CH_3COO_2)_2{\cdot}4H_2O$ $Ni(CH_3COO_2)_2{\cdot}4H_2O$, $Cu(CH_3COO_2)_2{\cdot}H_2O$, $Zn(CH_3COO_2)_2{\cdot}2H_2O$, coumarilic acid and 1,10-phenanthroline used in the synthesis of complexes were obtained from the company *Sigma-Aldrich*. Elemental analysis (C, H, N) was being carried out by standard methods.

Firstly, coumarilate salt compounds with natrium cation were synthesized by 0.005 mol of coumarilic acid dissolved in a 50:50 (v/v) $EtOH/H_2O$ solution in a beaker followed by the addition of 0.005 mol of $NaHCO_3$ providing CO_2 output. Then, the 1,10-phenanthroline solution (0.005 mol 25 mL H_2O) was first added to the salt solutions and mixed for 1 h in the magnetic stirrer. Finally, the metal–nitrate salts (0.0025 mol) in solid phase were appended to the main solution in 1:2 ratio concerning the coumarilate anion and mixed for 5 h at 60 °C (Scheme 2, Eq. 2).

The final solution was allowed to crystallize at atmospheric pressure by standing at room temperature. The crystals precipitated in approximately 20–30 days were collected by filtration. The metal/ligand/ligand ratio were considered as 1:2:2 for Co(II) and Ni(II) compounds and 1:2:1 for Cu(II) and Zn(II) compounds obtained.

Magnetic susceptibility measurements were taken at room temperature using a Sherwood Scientific MXI model Gouy magnetic balance. Infrared spectra were recorded in the 4000–400 cm^{-1} region with a PerkinElmer Spectrum One FTIR spectrophotometer using KBr pellets. (Approximately 0.03 grams of material was used for each pellet.) Thermal analyses (TG, DTA) were performed by the Shimadzu DTG-60H system, in a dynamic nitrogen atmosphere (100 mL min^{-1}) at a heating rate of 10 °C min^{-1}, in platinum crucibles as the sample vessel, using a-Al_2O_3 as a reference.

Structural characterizations of these synthesized complexes were characterized by elemental analysis, Fourier transforms infrared spectroscopy (FTIR), thermogravimetric analysis (TGA/DTA), single-crystal X-ray diffraction diffractometry (SC-XRD), solid-state ultraviolet–visible region spectroscopy (UV–Vis–NIR), magnetic susceptibility and melting point determination methods. The biologic activation studies of the elucidated molecules have been studied in cell culture medium.

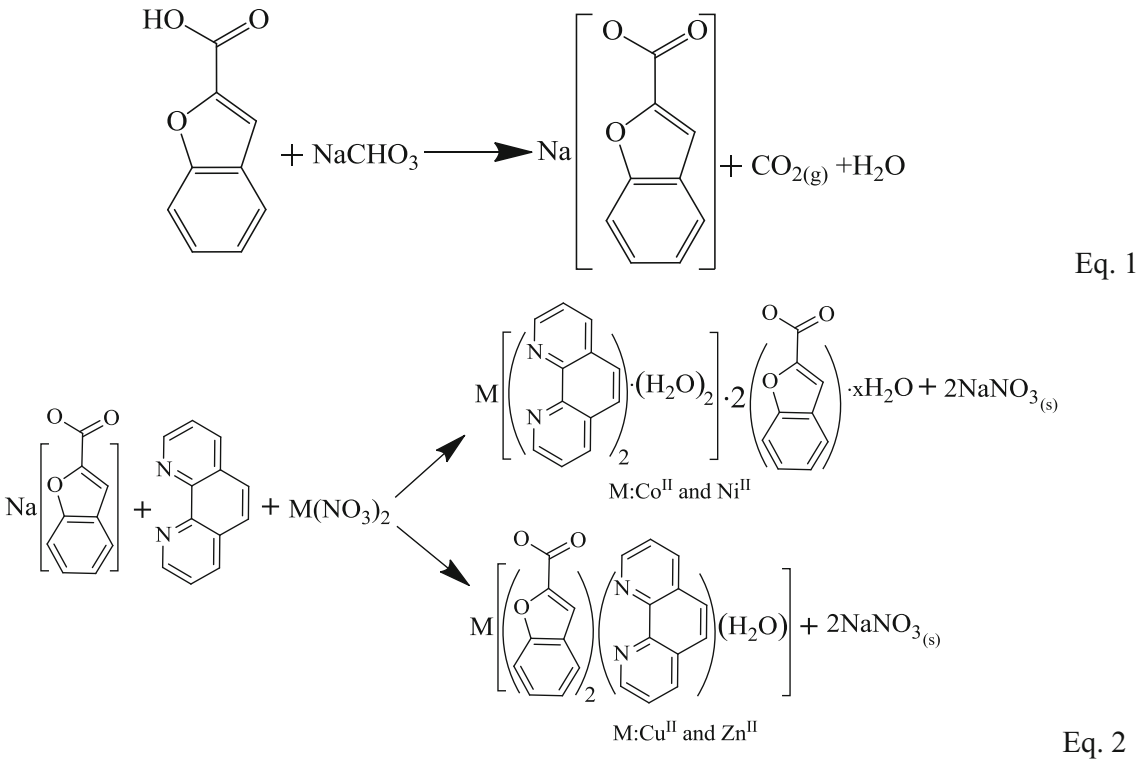

Scheme 2 Synthesis reaction of metal/coumarilate/1,10-phenanthroline coordination compounds

The antimicrobial effects of the elucidated molecules have been studied in Mueller–Hinton agar (MHA) medium as biological applications. Five different microorganisms were used in this study. These microorganisms were obtained from the culture collection of Molecular Biology and Genetics Department at Hitit University. One fungus (Candida albicans ATCC 10231), two gram-positive bacteria (Enterococcus faecalis ATCC 29212 and Staphylococcus aureus ATCC 6538) and two gram-negative bacteria (Pseudomonas aeruginosa ATCC 27853 and Escherichia coli ATCC 25922) were used as microorganisms.

The substances to be antimicrobial affected (0.001 g/10 mL) were prepared and passed through microfilters with a porosity of 0.45 μm and sterilized. 25-μL disks were adsorbed from the materials prepared using 10% DMSO (0.001 g substance/10 mL of 10% DMSO). 10% DMSO was used as a control. It was incubated for 24 h at 37 °C, and the inhibition zone diameters around the disks after incubation were measured as mm ± SD (standard deviation). Ampicillin and fluconazole antibiotic disks were used to compare the results with as standard.

Results and discussion

The elemental analysis data, decomposition points, magnetic susceptibility, colors and yield calculations of mixed ligand metal complexes are listed in Table 1.

FTIR analysis

The some important FTIR stretching and bending peaks of the complexes are summarized in Table 2, and the infrared curves are shown in Fig. 1. As the ligand of coumarilic acid in the synthesized complexes is bound to metal cations, a shift toward the right side is observed in the absorption bands corresponding to the functional groups. In the case of IR spectra, the strong and broadband observed around 3600–2900 cm^{-1} comes from the presence of the –OH group in the constructions of the complexes. The C=O group derived from the carboxylic acid group in the metal complexes gives stretching pulses of 1634 cm^{-1} for the Co(II) complex, 1608 cm^{-1} for the Ni(II) complex, 1611 cm^{-1} for the Cu(II) complex and 1616 cm^{-1} for the Zn(II) complex. The aromatic C=C tensile vibration is observed at 3060–3064 cm^{-1}. The aromatic C–H stretches in the complexes give stretching vibrations between 3373 and 3447 cm^{-1}. Carboxylic acid COO^{-} asymmetric and symmetrical absorption bands correspond to stretching

Table 1 Analytical data of metal complexes

Complex	M.W./g mol^{-1}	Yield/%	Content/% Exper. (Thero.)			Color	Decomp. temp./°C	$\mu_{eff.}$/BM
			C	H	N			
$[Co(C_{12}H_8N_2)_2(H_2O)_2](C_9H_5O_3)_2 5H_2O$	867.71	87	20.06	4.26	11.33	Purple	98	4.12
$C_{42}H_{40}CoN_4O_{13}$			(19.74)	(4.94)	(11.52)			
$[Ni(C_{12}H_8N_2)_2(H_2O)_2](C_9H_5O_3)_2 5H_2O$	867.49	94	20.01	4.67	11.61	Green	102	2.96
$C_{42}H_{40}N_4NiO_{13}$			(19.78)	(4.95)	(11.54)			
$[Cu(C_9H_5O_3)_2(C_{12}H_8N_2)(H_2O)]$	584.02	95	21.24	3.96	12.06	Blue	214	1.71
$C_{30}H_{20}CuN_2O_7$			(20.90)	(4.36)	(12.13)			
$[Zn(C_9H_5O_3)_2(C_{12}H_8N_2)(H_2O)]$	585.85	88	21.15	4.02	11.46	White	251	Dia.
$C_{30}H_{20}N_2O_7Zn$			(19.97)	(4.61)	(11.65)			

Table 2 FTIR spectra of metal–coumarilate–1,10-phenanthroline mixed ligand complexes

Groups	Co(II)	Ni(II)	Cu(II)	Zn(II)
$\nu(OH)_{H2O}$	3600–2800	3600–2800	3350–2900	3500–2900
$\nu(=C–H)_{ar}$	3377	3373	3447	3374
$\nu(C=C)_{ar}$	3064	3064	3060	3064
$\nu(C=O)_{karbonil}$	1634	1608	1611	1616
$\nu(COO–)_{asym}$	1556	1555	1559	1560
$\nu(COO–)_{sym}$	1388	1391	1389	1387
$\Delta\nu_{as\text{-}s}$	168	164	170	173
$\delta(OH)_{H_2O}$	1479	1480	1481	1481
$\nu(C–N–C)_{pyridin}$	1342	1338	1339	1340
$\nu(C_9–O_1–C_1)$	1249/1180	1253/1179	1250/1180	1250/1181
$\nu(C–O)_{carboxyl}$	1305	1304	–	–
ν(Ring)	1106–838	1105–845	1109–832	1107–838
ν(M–N)	588	583	576	588
$\nu(M–O)_{coumarilate}$	–	–	496	502
$\nu(M–O)_{H_2O}$	433	427	428	433

vibrations in the 1555–1560 cm^{-1} and 1387–139 cm^{-1} areas, respectively. The absorption bands corresponding to the metal–oxygen (M–O) bonds forming the basis of the complexes were observed for aqua ligands at 433 cm^{-1} in Co(II), 427 cm^{-1} in Ni(II), 428 cm^{-1} in Cu(II) and 433 cm^{-1} in Zn(II) complexes, respectively. Also, just two complexes have (M–O) bonds stretching vibrations for the coumarilate ligand, Cu(II) and Zn(II) complexes, so coumarilate ligands were coordinated to metal cations in these compounds. But in the other two complexes are the salt type, so the anionic coumarilate ligands did not coordinate to metal, Co(II) and Ni(II), cations. The vibrations of the metal–nitrogen (M–N) bonds in the complex are

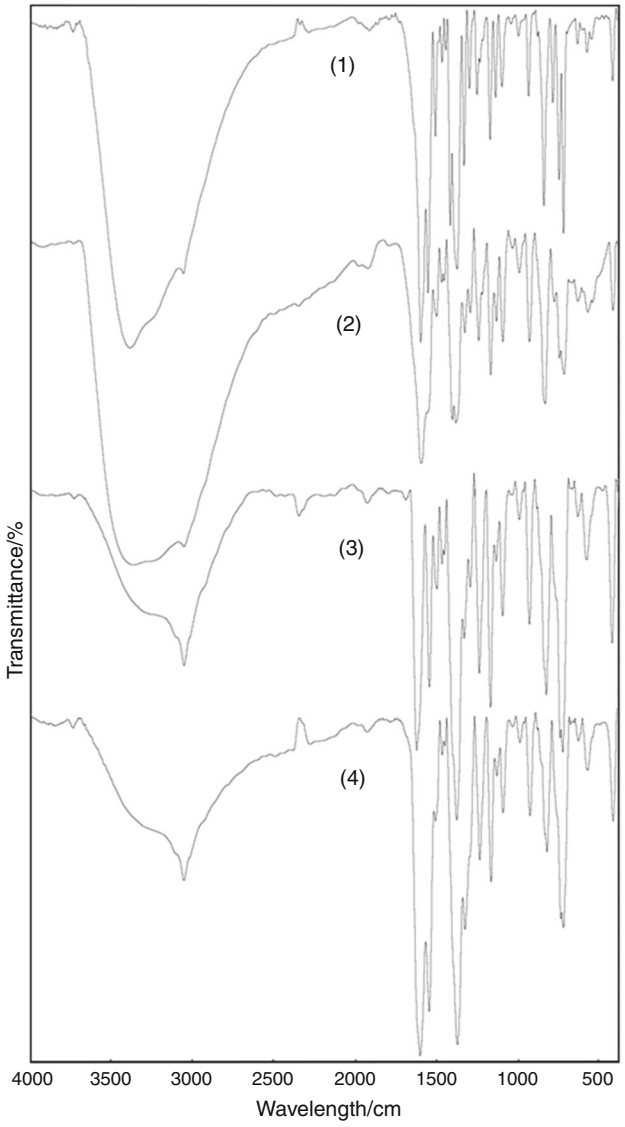

Fig. 1 The FTIR curves of complexes, for Co(II) is **(1)**, for Ni(II) is **(2)**, for Cu(II) is **(3)** and for Zn(II) is **(4)**

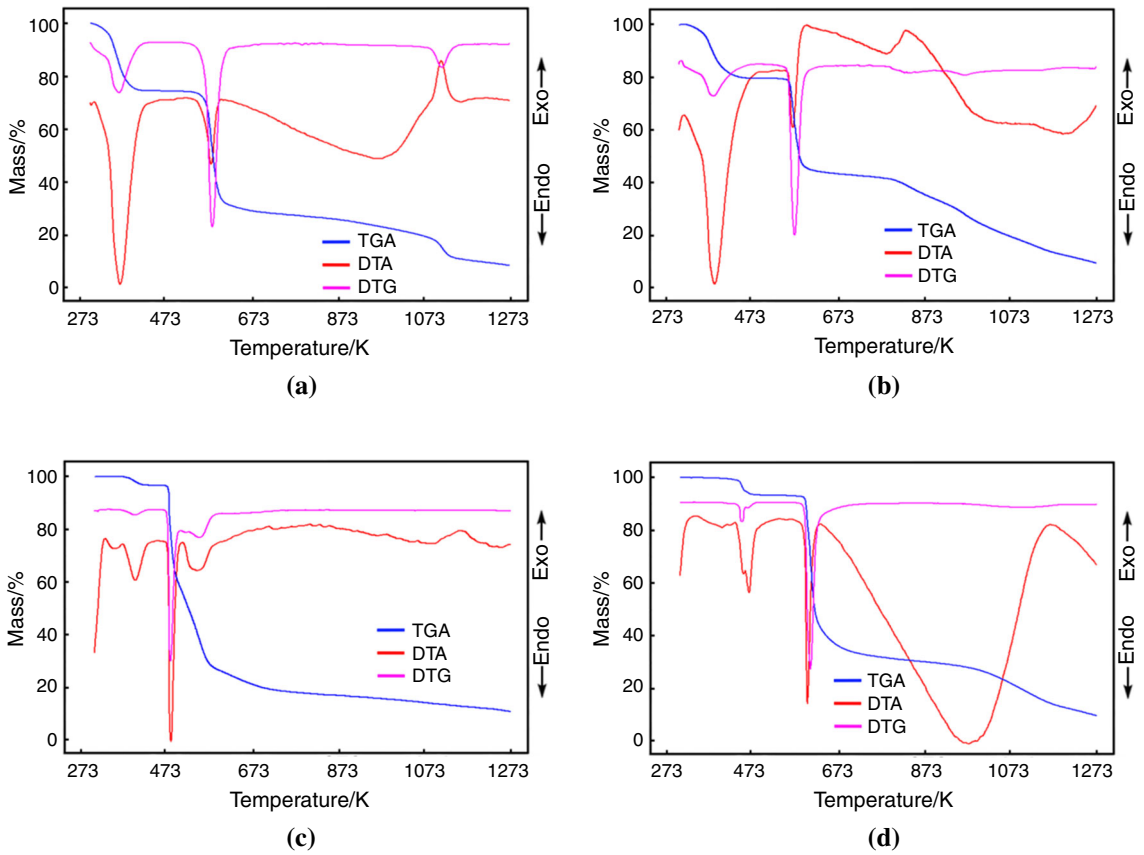

Fig. 2 Thermal analysis curves of molecules **a** Co(II) complex, **b** Ni(II) complex, **c** Cu(II) complex and **d** Zn(II) complex

588 cm^{-1} for the Co(II) complex, 583 cm^{-1} for the Ni(II) complex, 576 cm^{-1} for Cu(II) complex and 588 cm^{-1} for Zn(II) complex.

Thermal properties

The curves of TG, DTG and DTA for thermal characterization of complexes are shown in Fig. 2a–d. The details of the decomposition steps are listed in Table 3.

When the Co(II) mixed ligand complex is examined on the DTG curve, thermal degradation occurs in four steps. The initial temperatures of the decays were determined as 40, 70, 237 and 332 °C. In the first decay step, it is thought that a molar water ligand has been removed from the structure.

$$[Co(C_{12}H_8N_2)_2(H_2O)_2](C_9H_5O_3)_2 \cdot 5H_2O_{(s)} \overset{40-69\,^{\circ}C}{\longrightarrow} [Co(C_{12}H_8N_2)_2(H_2O)_2](C_9H_5O_3)_2 \cdot 4H_2O_{(s)} + H_2O_{(g)}. \quad (R.1)$$

At the temperature range of 70–147 °C, the remained six moles (2 mol coordination and 4 mol hydrated water) of the aqua ligands are completely separated from the structure at the 93 °C dehydration step.

$$[Co(C_{12}H_8N_2)_2(H_2O)_2](C_9H_5O_3)_2 \cdot 4H_2O_{(s)} \overset{70-147\,^{\circ}C}{\longrightarrow} [Co(C_{12}H_8N_2)_2](C_9H_5O_3)_{2(s)} \cdot 6H_2O_{(g)}. \quad (R.2)$$

Two moles of 1,10-phenanthroline ligand and two moles of the coumarilate ligand are degraded in the temperature range of 237–863 °C. As a decomposition product, there remains a black CoO compound.

$$[Co(C_{12}H_8N_2)_2](C_9H_5O_3)_{2(s)} \overset{237-863\,^{\circ}C}{\longrightarrow} CoO_{(s)} + 2C_{12}H_8N_{2(decomp)} + 2C_9H_5O_{3(decomp)}. \quad (R.3)$$

The DTG curve complex of the Ni(II) mixed ligand complex 54, 97, 260; 459, 644 and 831 °C, corresponding to the maximum temperatures. In the first decay step (at 37–70 °C), 1 mol of water ligand is moving away from the structure.

$$[Ni(C_{12}H_8N_2)_2(H_2O)_2](C_9H_5O_3)_2 \cdot 5H_2O_{(s)} \overset{37-70\,^{\circ}C}{\longrightarrow} [Ni(C_{12}H_8N_2)_2(H_2O)_2](C_9H_5O_3)_2 \cdot 4H_2O_{(s)} + H_2O_{(g)}. \quad (R.4)$$

Similar to Co(II) complex, at the temperature range of 71–164 °C, all remaining aqua ligands (6 mol) are

Table 3 Thermoanalytical data (TG-DTG/DTA) for the metal complexes

Complex	Temp. range/°C	DTA_{max}/°C	Withdrawing group	Mass loss/%		Residue/%		Decomp. product	Color
				Exp.	Theor.	Exp.	Theor.		
$[Co(C_{12}H_8N_2)_2(H_2O)_2](C_9H_5O_3)_2 5H_2O$									Purple
$C_{42}H_{40}CoN_4O_{13}$									
867.71 g/mol									
1	40–69	55	H_2O	2.12	2.08				
2	70–147	93	$6H_2O$	13.01	12.45				
3	237–330	282	$2C_{12}H_8N_2$	39.67	41.49				
4	332–863	626, –759	$C_9H_5O_2$; $C_9H_5O_3$	34.71	35.29	10.49	8.64	CoO	Black
$[Ni(C_{12}H_8N_2)_2(H_2O)_2](C_9H_5O_3)_2 5H_2O$									Green
$C_{42}H_{40}N_4NiO_{13}$									
867.49 g/mol									
1	37–70	54	H_2O	2.25	2.08				
2	71–164	97	$6H_2O$	13.34	12.45				
3	235–308	260	$2C_{12}H_8N_2$	40.38	41.50				
4	310–877	459, 644, 831	$C_9H_5O_2$; $C_9H_5O_3$	33.96	35.30	10.07	8,61	NiO	Black
$[Cu(C_9H_5O_3)_2(C_{12}H_8N_2)(H_2O)]$									Blue
$C_{30}H_{20}CuN_2O_7$									
584.02 g/mol									
1	102–150	127	H_2O	2.98	3.08				
2	191–211	201	$C_{12}H_8N_2$	30.14	30.82				
3	212–743	257	$C_9H_5O_2$; $C_9H_5O_3$	50.67	52.44	16.21	13.62	CuO	Black
$[Zn(C_9H_5O_3)_2(C_{12}H_8N_2)(H_2O)]$									White
$C_{30}H_{20}N_2O_7Zn$									
585.85 g/mol									
1	144–186	158, 170	H_2O	3.64	3.07				
2	277–311	293	$C_{12}H_8N_2$	30.95	30.72				
3	312–821	624	$C_9H_5O_2$; $C_9H_5O_3$	50.88	52.27	14.53	13.89	ZnO	Gray

completely got away from the structure as a decomposition step.

$$[Ni(C_{12}H_8N_2)_2(H_2O)_2](C_9H_5O_3)_2 \cdot 4H_2O_{(s)} \overset{71-164\,^{\circ}C}{\longrightarrow} [Ni(C_{12}H_8N_2)_2](C_9H_5O_3)_{2(s)} + 6H_2O_{(g)}. \quad (R.5)$$

Two moles of 1,10-phenanthroline ligand and two moles of coumarilate ligand decay in the temperature range 235–877 °C, leaving the medium. As a decay product, there remains a black NiO compound.

$$[Ni(C_{12}H_8N_2)_2](C_9H_5O_3)_{2(s)} \overset{235-877\,^{\circ}C}{\longrightarrow} NiO_{(s)} + 2C_{12}H_8N_{2(decomp)} + 2C_9H_5O_{3(decomp)}. \quad (R.6)$$

The Cu(II) coordination compound exhibits three decomposition steps. These steps start at the 102, 191 and 212 °C, and the first degradation step can be attributed to the removal of one-mole aqua ligand in the coordination sphere from the structure.

$$[Cu(C_9H_5O_3)_2(C_{12}H_8N_2)(H_2O)_2]_{(s)} \overset{102-150\,^{\circ}C}{\longrightarrow} [Cu(C_9H_5O_3)_2(C_{12}H_8N_2)]_{(s)} + H_2O_{(g)}. \quad (R.7)$$

At the temperature range of 191–743 °C, two molecules of 1,10-phenanthroline ligand, which is the organic structure of coordination complex, and two moles of coumarilate ligands burn away from the medium. As the last product, there remains a black CuO compound.

Table 4 Crystal data and structure refinement parameters for complexes **1**–**4**

Crystal data	**1**	**2**	**3**	**4**
Empirical formula	$C_{42}H_{40}CoN_4O_{13}$	$C_{42}H_{40}NiN_4O_{13}$	$C_{30}H_{20}CuN_2O_7$	$C_{30}H_{20}ZnN_2O_7$
Formula weight	867.71	867.49	584.02	585.85
Crystal system	Monoclinic	Monoclinic	Triclinic	Triclinic
Space group	$P2_1/c$	$P2_1/c$	P-1	P-1
a/Å	13.2078 (8)	13.1870 (9)	7.8374 (5)	7.8628 (4)
b/Å	22.3117 (12)	22.2182 (16)	10.8634 (7)	10.9545 (6)
c/Å	15.3660 (9)	15.3943 (12)	16.1168 (11)	15.8450 (9)
α/°	90.00	90.00	100.405 (2)	101.091 (2)
β/°	112.200 (2)	112.075 (2)	94.592 (3)	94.371 (3)
γ/°	90.00	90.00	109.952 (2)	107.883 (2)
V/Å^3	4192.5 (4)	4179.8 (5)	1253.64 (14)	1261.14 (12)
Z	4	4	2	2
D_c/g cm^{-3}	1.375	1.379	1.547	1.543
θ range/°	3.0–22.7	3.1–27.0	3.1–28.2	3.5–28.3
Measured refls.	116,218	84,594	64,581	56,939
Independent refls.	7793	8196	6288	6268
R_{int}	0.114	0.062	0.040	0.036
S	1.42	1.59	1.16	1.16
R1/wR2	0.117/0.375	0.110/0.391	0.037/0.106	0.038/0.093
$\Delta\rho_{max}/\Delta\rho_{min}$/eÅ^{-3}	1.32/− 1.46	2.27/− 0.76	0.32/− 0.60	0.62/− 0.55

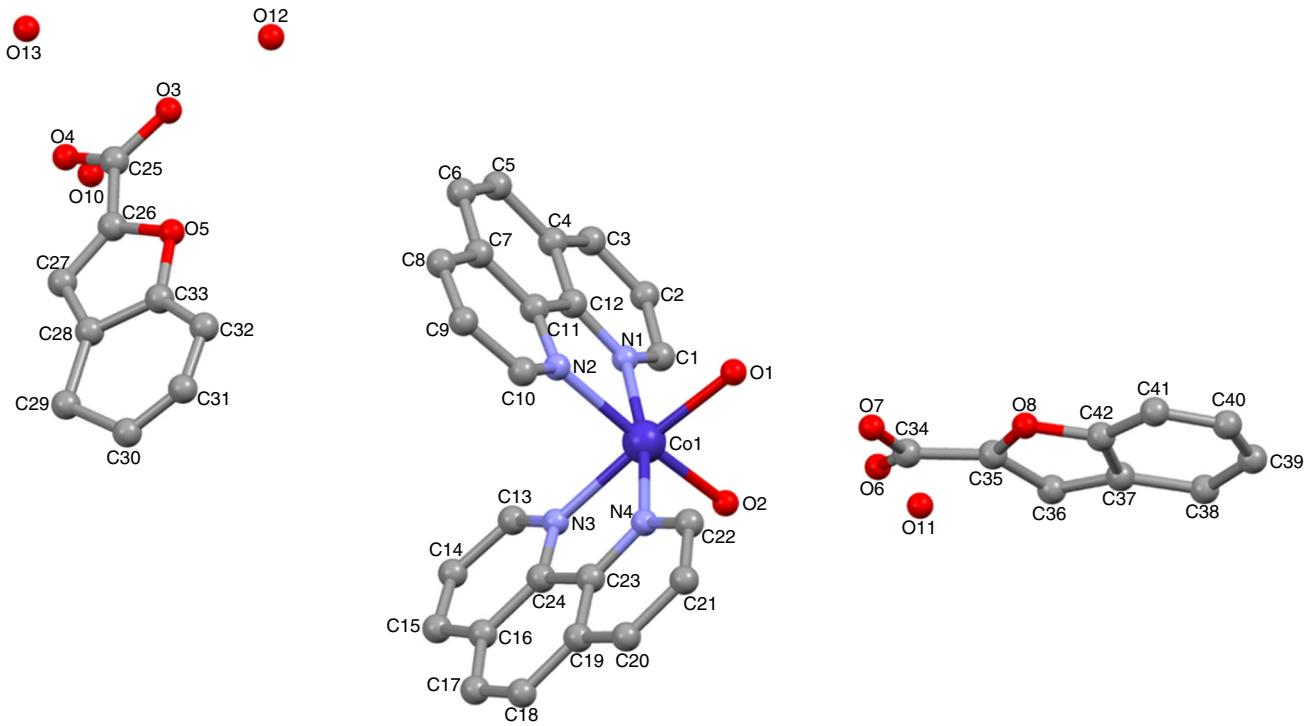

Fig. 3 The molecular structure of complex **1** showing the atom-numbering scheme

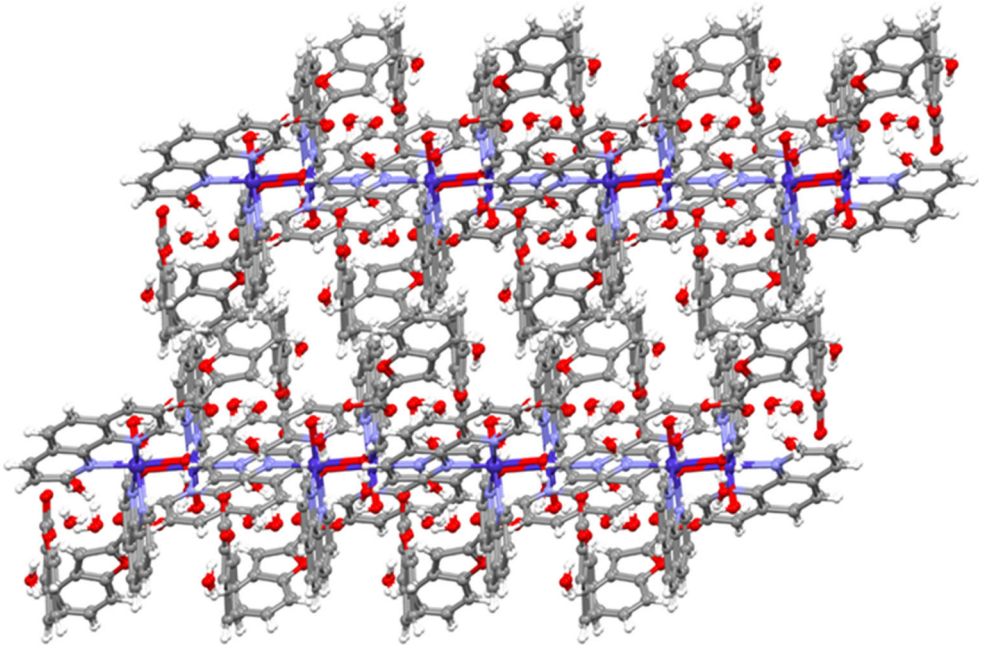

Fig. 4 The 3D supramolecular network in **1**

Table 5 Selected bond distances and angles for complexes **1**–**4** (Å, °)

Complex **1**					
Co1–O2	2.074 (5)	Co1–N2	2.141 (5)	Co1–N3	2.140 (5)
Co1–O1	2.091 (7)	Co1–N4	2.146 (5)	Co1–N1	2.157 (5)
O2–Co1–O1	89.5 (3)	O2–Co1–N3	90.2 (2)	O1–Co1–N3	173.3 (3)
O2–Co1–N2	169.9 (2)	O1–Co1–N2	91.7 (2)	O2–Co1–N4	94.5 (2)
Complex **2**					
N1–Ni1	2.093 (5)	N2–Ni1	2.091 (4)	N3–Ni1	2.079 (5)
N4–Ni1	2.093 (5)	Ni1–O2	2.059 (5)	Ni1–O1	2.063 (5)
O2–Ni1–O1	89.4 (2)	O2–Ni1–N3	89.98 (19)	O1–Ni1–N3	175.3 (2)
O2–Ni1–N2	92.4 (2)	O1–Ni1–N2	88.7 (2)	N3–Ni1–N2	96.04 (18)
Complex **3**					
N1–Cu1	2.0244 (17)	N2–Cu1	2.0032 (17)	O1–Cu1	2.2872 (15)
O4–Cu1	1.9367 (15)	Cu1–O7	1.9864 (15)		
O4–Cu1–O7	94.60 (7)	O4–Cu1–N2	89.17 (6)	O7–Cu1–N1	92.12 (7)
O4–Cu1–O1	99.07 (7)	O7–Cu1–O1	92.84 (6)	N1–Cu1–O1	89.01 (6)
Complex **4**					
O1–Zn1	2.0316 (16)	O4–Zn1	1.9972 (16)	Zn1–O7	2.062 (2)
Zn1–N2	2.0981 (17)	Zn1–N1	2.1543 (18)		
O4–Zn1–O1	102.69 (7)	O7–Zn1–N2	141.18 (11)	O4–Zn1–N1	96.76 (7)
O1–Zn1–N1	159.13 (7)	O7–Zn1–N1	89.81 (8)	N2–Zn1–N1	78.35 (7)

$$[Cu(C_9H_5O_3)_2(C_{12}H_8N_2)]_{(s)} \xrightarrow{191-743\,^{\circ}C} CuO_{(s)} + 2C_9H_5O_{3(decomp)} + C_{12}H_8N_{2(decomp)}. \quad (R.8)$$

The Zn(II) complex also degrades at the three decomposition stages (114; 277 and 312 °C), as is the case in the Cu(II) complex structure. The first disruption step in the range 144–186 °C is due to the removal of one-mole aqua ligand in the coordination cage.

$$[Zn(C_9H_5O_3)_2(C_{12}H_8N_2)(H_2O)]_{(s)} \xrightarrow{144-186\,^{\circ}C} [Zn(C_9H_5O_3)_2(C_{12}H_8N_2)]_{(s)} + H_2O_{(g)}. \quad (R.9)$$

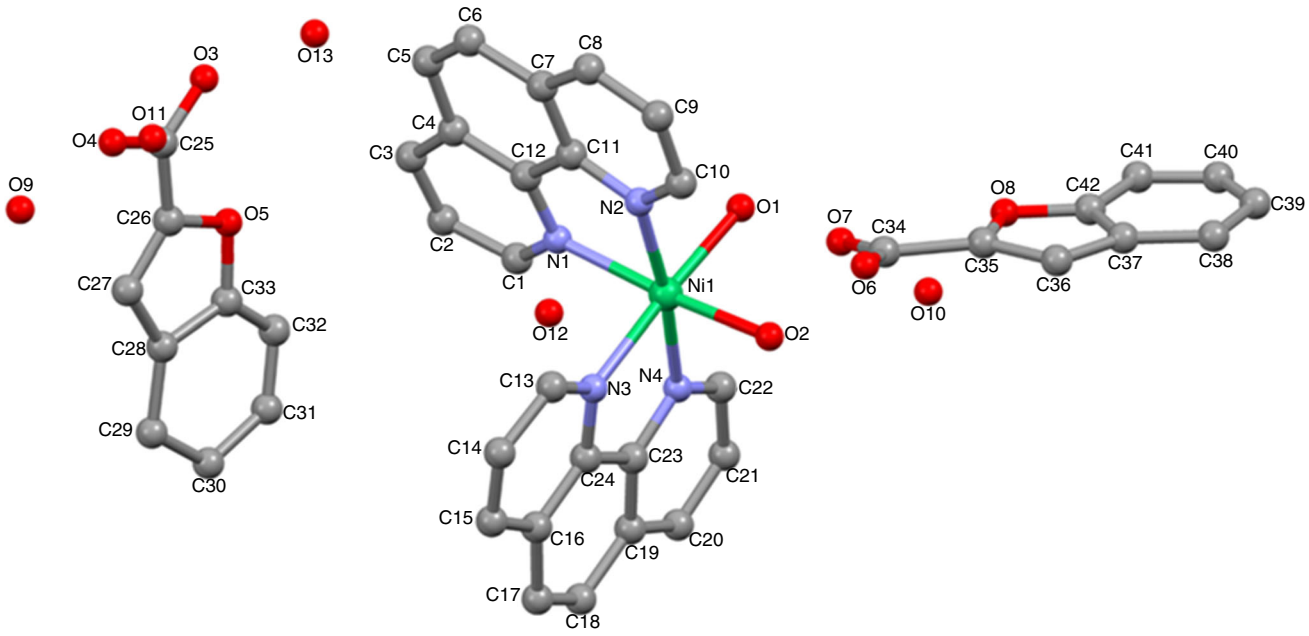

Fig. 5 The molecular structure of complex **2** showing the atom-numbering scheme

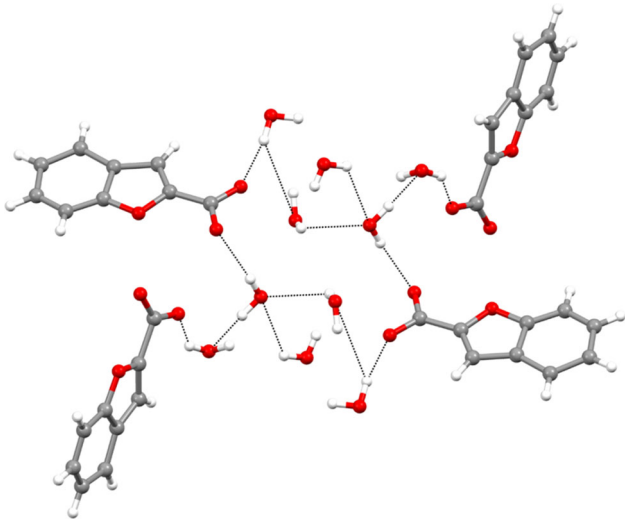

Fig. 6 The formation of $R_8^8(16)$ ring in **2**

The dehydrated complex structure burns at a temperature range of 277–821 °C. In this step, the two moles of 1,10-phenanthroline and two moles of the coumarilate ligands are separated from the structure by forming possible $CO_2/CO_2/NO_2/NO_2$ gases as they are in other structures. Leaving behind the gray colored ZnO compound remained in the reaction crucible as the final decomposition product.

$$[Zn(C_9H_5O_3)_2(C_{12}H_8N_2)]_{(s)} \xrightarrow{277-821\,^{\circ}C} ZnO_{(s)} + 2C_9H_5O_{3(decomp)} + C_{12}H_8N_{2(decomp)}. \quad (R.10)$$

All remaining relevant oxides were investigated with IR spectra, and the claim was supported.

X-ray diffraction analysis

Suitable crystals of $C_{42}H_{40}CoN_4O_{13}$ (**1**), $C_{42}H_{40}N_4NiO_{13}$ (**2**), $C_{30}H_{20}CuN_2O_7$ (**3**) and $C_{30}H_{20}N_2O_7Zn$ (**4**) were selected for data collection which was performed on a Bruker APEX-II diffractometer equipped with graphite-monochromatic Mo-K_α radiation. The structures were solved by direct methods using SHELXS-97 [20] and refined by full-matrix least-squares methods on F^2 using SHELXL-97 [20] from within the WINGX [21] suite of software. All non-hydrogen atoms were refined with anisotropic parameters. The H atoms of C atoms were located from different maps and then treated as riding atoms with C–H distances of 0.93 Å. The water H atoms were located in a difference map refined freely. Molecular diagrams were created using MERCURY [22]. Supramolecular analyses were performed, and the diagrams were prepared with the aid of PLATON [23]. Details of data collection and crystal structure determinations are given in Table 4.

Complexes 1 and 2

The molecular structures of complexes **1**–**2**, with the atom-numbering schemes, are shown in Figs. 3 and 4. The asymmetric units of **1**–**2** contain one M(II) ion (M(II) = Co(II) in **1** and Ni(II) in **2**), two phenanthroline ligands,

Table 6 Hydrogen-bond parameters for complexes **1–4** (Å, °)

D–H···A	D–H	H···A	D···A	D–H···A
Complex **1**				
C2–H2···O10^{i}	0.93	2.50	3.240 (14)	137
C10–H10···O5^{ii}	0.93	2.53	3.204 (9)	130
O1–H1B···O7	0.80 (11)	1.87 (12)	2.594 (12)	149
O2–H2A···N3	0.79 (10)	2.52 (10)	2.984 (7)	120
O2–H2B···O6	0.90 (7)	1.85 (7)	2.696 (10)	156
O9–H9B···O4	0.87	1.93	2.790 (13)	169
O10–H10B···O4	0.99	1.76	2.750 (12)	176
O11–H11A···O6	0.84	1.66	2.36 (2)	140
Complex **2**				
C1–H1···O5^{i}	0.93	2.52	3.188 (8)	129
C9–H9···O11^{ii}	0.93	2.46	3.230 (14)	141
O1–H1A···O10^{iii}	0.82 (2)	1.87 (3)	2.673 (13)	167
O1–H1B···O7	0.82 (2)	1.87 (5)	2.607 (11)	148
O2–H2A···O6	0.83 (2)	1.91 (3)	2.693 (10)	156
O2–H2B···O3^{iv}	0.83 (2)	2.10 (9)	2.664 (9)	126
O9–H9A···O4	0.92	1.92	2.823 (12)	169
O10–H10A···O6	0.80	1.76	2.41 (2)	138
O13–H13B···O10^{v}	0.87	2.08	2.83 (3)	144
O13–H13A···O3	0.83	2.11	2.68 (2)	125
Complex **3**				
C3–H3···O4^{i}	0.93	2.58	3.417 (3)	150
O7–H7A···O1^{ii}	0.80 (2)	2.54 (2)	3.322 (4)	166
O7–H7B···O2	0.84 (2)	1.85 (2)	2.654 (3)	161
Complex **4**				
C12–H12···O1^{i}	0.93	2.53	3.352 (2)	148
O7–H7A···O5	0.83 (2)	1.84 (2)	2.642 (2)	163
O7–H7B···O2	0.84 (2)	1.73 (2)	2.552 (3)	163

Symmetry codes: (i) $-x+1, -y+1, -z+1$; (ii) $x, -y+1/2, z+1/2$ for **1**; (i) $x, -y+3/2, z-1/2$; (ii) $-x+1, -y+1, -z+1$; (iii) $x, -y+3/2, z+1/2$; (iv) $x, y, z-1$; (v) $x, y, z+1$ for **2;** (i) $-x+1, -y+1, -z+1$; (ii) $-x, -y+1, -z+1$ for **3**; (i) $-x+1, -y+1, -z+1$ for **4**

two non-coordinated coumarilate ligands, five non-coordinated water molecules and two aqua ligands. Each M(II) ion is coordinated by four nitrogen atoms of two different phenanthroline ligands and two oxygen atoms from aqua ligands. The coordination geometry around the M(II) cation can be described as a distorted octahedral geometry. The M–O bond lengths are 2.074 (5) and 2.091 (7) Å in **1** and 2.059 (5) and 2.063 (5) Å in **2**, respectively. The M–N bond lengths are ranged between 2.140 (5)–2.157 (5) Å in **1** and 2.079 (5)–2.093 (5) Å in **2**, respectively (Table 5). The 3D supramolecular network of molecules is shown in Fig. 5 for complex **1** and Fig. 6 for complex **2**.

Molecules of **1** are linked by C–H···O hydrogen bonds, while molecules of **2** are linked into sheets by a combination of O–H···O and C–H···O hydrogen bonds (Table 6). In **2**, strong hydrogen bonds are observed between coumarilate ligands and water oxygen atoms, with the O···O distances ranging from 2.664 (9) to 2.83 (3) Å. The combination of O–H···O hydrogen bonds produces $R_8^8(16)$ ring (Fig. 7). All of these intermolecular interactions give three-dimensional framework results.

Complexes 3 and 4

The molecular structures of complexes **3–4**, with the atom-numbering scheme, are shown in Fig. 8. The asymmetric units of **3–4** contain one M(II) cation, one phenanthroline ligand, two coumarilate ligands and one aqua ligand. Each M(II) ion is coordinated by two nitrogen atoms of phenanthroline ligand, two oxygen atoms of two different coumarilate ligands and one oxygen atom from the aqua ligand. The coordination geometry around the M(II) cation can be described as a distorted square pyramidal geometry. The M–$O_{carboxyl}$ bond lengths are 1.9367 (15) and 2.2872 (15) Å in **3** and 1.9972 (16) and 2.0316 (16) Å in **4**, while the M–O_{aqua} bond length is 1.9864 (15) Å in **3** and 2.062 (2) Å in **4**, respectively. The M–N bond lengths are 2.0032 (17) and 2.0244 (17) Å in **3** and 2.0981 (17) and 2.1543 (18) Å in **4**, respectively (Table 5).

Molecules of **4** are linked by a combination of O–H···O and C–H···O hydrogen bonds, while molecules of **3** are linked by C–H···O hydrogen bond (Table 6). In **4**, atom C3 atom in the molecule at (x, y, z) acts as hydrogen-bond donor, via atom H3, to atom O4^{i}, so forming a centrosymmetric $R_2^2(14)$ ring centered at $(n + 1/2, 1/2, 1/2)$ [n = zero or integer] [(i) $-x+1, -y+1, -z+1$]. Similarly, water O7 atom in the molecule at (x, y, z) acts as hydrogen-bond donor, via atom H7A, to atom O1^{ii}, so forming centrosymmetric $R_2^2(8)$ ring centered at $(n, 1/2, 1/2)$ [n = zero or integer] [(ii) $-x, -y+1, -z+1$]. The combination of these hydrogen bonds produces edge-fused $R_2^2(8)R_2^2(14)$ rings which is running parallel to the [010] direction (Fig. 9). In **3**, atom C12 atom in the molecule at (x, y, z) acts as hydrogen-bond donor, via atom H12, to atom O1^{i}, so forming a centrosymmetric $R_2^2(14)$ ring centered at (1/2, 1/2, 1/2) [(i) $-x+1, -y+1, -z+1$].

The solid-state UV–Vis spectroscopy

Electronic transition values were subtracted from the spectral patterns of the synthesized metal–coumarilate–1,10-phenanthroline mixed ligand complexes according to the visible region spectroscopy (UV–Vis) recorded at 900–200 nm (Fig. 10). The electronic transition peaks are listed in Table 7. According to these results, the *d–d* transitions of the Co(II) complex are seen at wavelengths of 632.21 nm ($^4T_{1g} \rightarrow {}^4T_{2g}$)(F) and 533.27 nm ($^4T_{1g} \rightarrow {}^4T_{1g}$)(P). The three spin-permuted d–d passages possessed

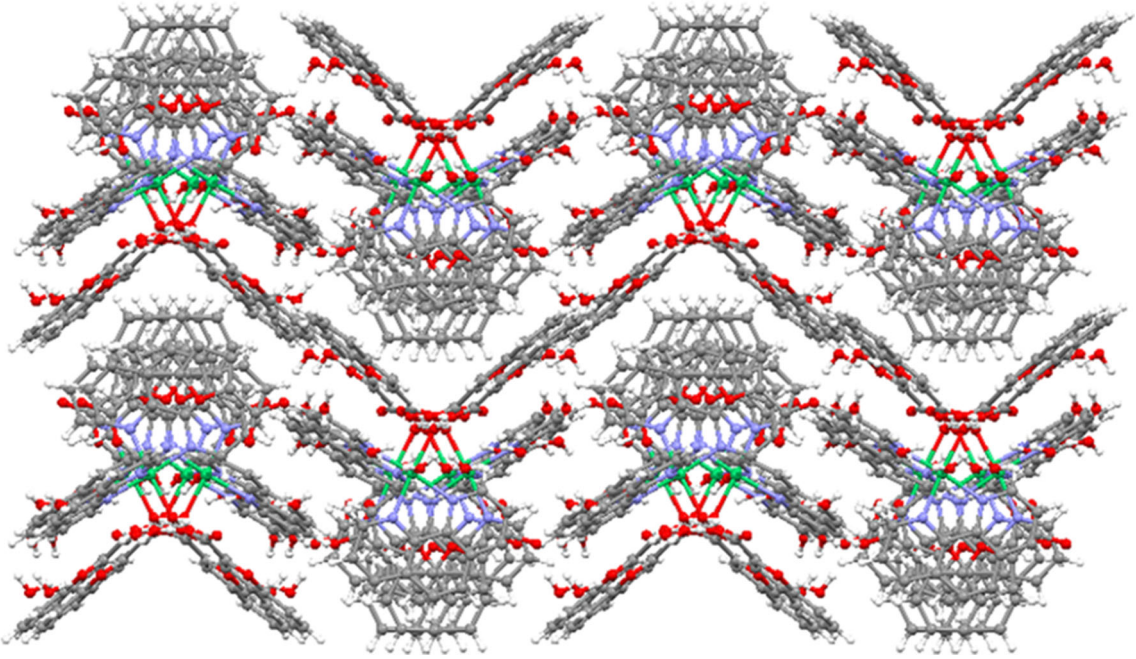

Fig. 7 The 3D supramolecular network in **2**

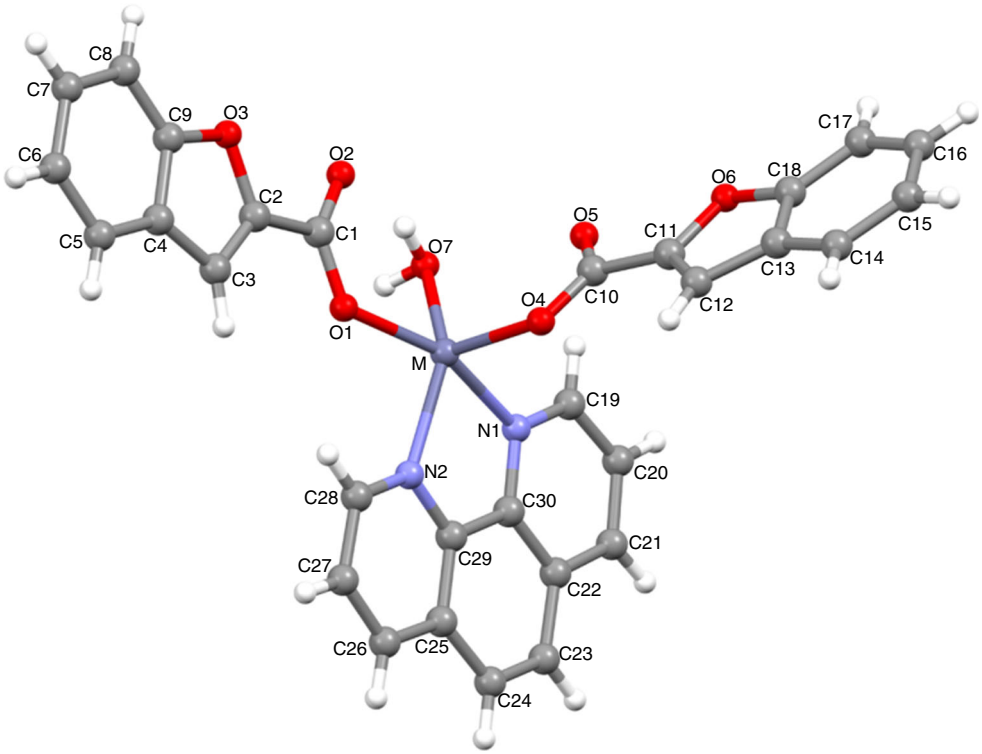

Fig. 8 The molecular structure of complexes **3**–**4** (*M* = Cu(II) in **3** and Zn(II) in **4**) showing the atom-numbering scheme

by the Ni(II) complex were found to be 815.03 nm ($^3A_{2g} \rightarrow {}^3T_{1g}$)(P), 607.71 nm ($^3A_{2g} \rightarrow {}^3T_{1g}$)(F) and 441.26 nm ($^3A_{2g} \rightarrow {}^3T_{2g}$)(F) wavelengths, which indicate the splitting of the d orbitals of the Ni(II) metal cation to support the octahedral geometry.

The spectrum for the Cu(II) complex is similar to the electronic transitions in other Cu(II) complexes in the literature [14, 15], but the peak intensity is higher. (This is seen when complexes of Cu(II) metal cations are compared.) So, the copper metal cation has a single electronic transition similar to the structure in the pseudo-octahedral,

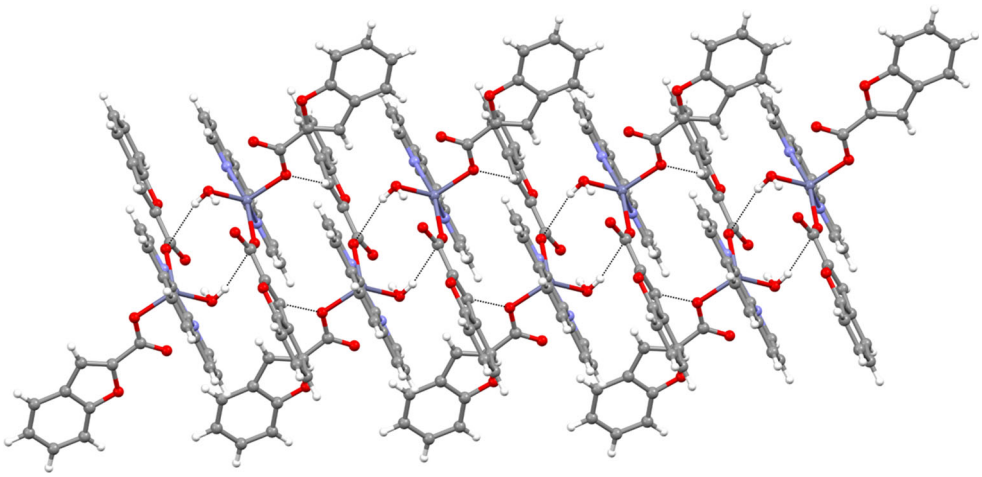

Fig. 9 The formation of edge-fused $R_2^2(8)R_2^2(14)$ rings in **3**

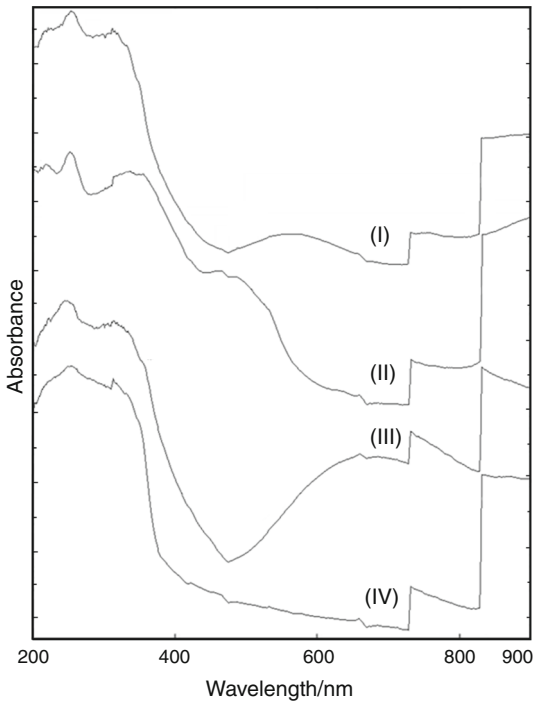

Fig. 10 UV–Vis–NIR spectra of complexes **1–4**

but that the energy difference between the bands with the transition is higher. For this reason, the transition can be attributed to the passage of the square pyramidal structure ($A_{1g} \rightarrow B_{1g}$). The structure analyzed by single-crystal XRD results supports UV–Vis results. As shown in the magnetic susceptibility results, there is no *d–d* electron transition in the square pyramidal splitting which can occur when the orbitals in the last orbit of the metal cation in the Zn(II) complex, which has the diamagnetic property, are fully charged.

The absorption band seen at a low wavelength with high severity does not belong to the *d–d* transition, but the stronger energy metal → ligand (M → L) belongs to the charge transfer transition. Absorption bands at wavelengths of 247,38 and 311,11 nm for Co(II) complex, 249,77 and 325,41 nm for Ni(II) complex, 238,15 and 308,42 nm for Cu(II) complex, respectively, belong to metal → ligand (M → L transitions. The strong DTGs at the wavelengths of 247.17 and 311.23 nm for the Zn(II) complex belong to ligand → metal (L → M) charge transfer. All of the solid-phase data of metal cation complexes are suitable for the literature [24–26].

Table 7 The UV–Vis spectra of metal–coumarilate mixed ligand complexes

Transitions	Complexes			
	$C_{42}H_{40}CoN_4O_{13}$ (octahedral)	$C_{42}H_{40}N_4NiO_{13}$ (octahedral)	$C_{30}H_{20}CuN_2O_7$ (square pyramidal)	$C_{30}H_{20}N_2O_7Zn$ (square pyramidal)
d–d	632,21 ($^4T_{1g} \rightarrow {}^4T_{2g}$)(F)	815,03 ($^3A_{2g} \rightarrow {}^3T_{1g}$)(P)	852,56–496,13 631,92 ($A_{1g} \rightarrow B_{1g}$)	–
d–d	533,27 ($^4T_{1g} \rightarrow {}^4T_{1g}$)(P)	607,71 ($^3A_{2g} \rightarrow {}^3T_{1g}$)(F)		
d–d		441,26 ($^3A_{2g} \rightarrow {}^3T_{2g}$)(F)		
M→L	247,38; 311,11	249,77; 325,41	238,15; 308,42	–
L → M	–	–	–	247,17; 311,23

Table 8 Some biological applications results of complexes

Samples	*Staphylococcus aureus*	*Enterococcus faecalis*	*Escherichia coli*	*Pseudomonas aeruginosa*	*Candida albicans*
Antimicrobial activity (inhibition diameter, mm ± SD)					
Complex **1**	ND	5.0 ± 1.0	3.0 ± 0.5	ND	6.0 ± 1.0
Complex **2**	ND	ND	1.0 ± 0.5	1.0 ± 0.5	4.0 ± 1.5
Complex **3**	1.0 ± 0.5	1.0 ± 0.5	3.0 ± 1.0	ND	5.0 ± 2.0
Complex **4**	2.0 ± 1.0	ND	2.0 ± 0.5	1.0 ± 0.5	6.5 ± 2.0
Standard[a]	7.00 ± 1.00	9.50 ± 2.00	10.50 ± 2.50	8.75 ± 2.25	ND
Standard[b]	ND	ND	ND	ND	10.50 ± 1.50

ND not determined, Standard[a]: ampicillin, Standard[b]: fluconazole

Biological applications

The antimicrobial (antibacterial, antifungal) activity of the synthesized complexes is given in Table 8.

Co(II) complex was found to be effective on *Candida albicans* and also low inhibition effect on *Enterococcus faecalis* and *Escherichia coli*. Ni(II) complex was found to be effective in *Candida albican*s and also the low inhibitory effect on Gram-negative microorganisms (*Escherichia coli* and *Pseudomonas aeruginosa*). Cu(II) complex was found to be effective on *Candida albicans* and also low inhibition effect on *Staphylococcus aureus*, *Enterococcus faecalis* and *Escherichia coli*. Zn(II) complex was found to be effective in *Candida albicans,* and a low rate of inhibition was also found in *Staphylococcus aureus*, *Escherichia coli* and *Pseudomonas aeruginosa*.

Conclusions

The mixed ligand complexes of cobalt (II), nickel (II), copper (II) and zinc (II) metal cation were synthesized with coumarilic acid and 1,10-phenanthroline ligands. The ratio of metal/coumarilate/1,10-phenanthroline ligands was determined as 1:2:2 in Co(II) and Ni(II) complexes and 1:2:1 in Cu(II) and Zn(II) complexes. The Co(II) and Ni(II) cations in the structures have completed their octahedral sphere with two moles bidentate bonded 1,10-phenanthroline and two moles aqua as a ligand by entering the coordination sphere. The both of the structures include four moles hydrated water molecules but they are not isostructural, so the water molecules outside of the coordinate system are located in different spatial regions. According to the structural analysis results obtained, the complexes of **3** and **4**, whose structure was identified, were determined as isostructural and their coordination modes are square pyramidal. The complexes of **1** and **2** are salt type, and two moles coumarilate anions are settled outside of the coordination spheres that are counter-ions of metal cations. **1** and **2** are similar to each other because their thermal degradation steps are similar to each other, whereas structures **3** and **4** are isostructures, the same. The biological activation studies of the elucidated molecules have been studied in cell culture medium. Synthesized molecules have been found to have higher activity, especially against Candida albicans fungus. It has been observed that these activities are close to the effect of gentamicin and fluconazole drugs present in the market.

Supplementary material

Crystallographic data for the structural analysis have been deposited with the Cambridge Crystallographic Data Centre, CCDC No. 1468909 for **1**, 1468910 for **2**, 1468911 for **3** and 1468912 for **4**. Copies of this information may be obtained free of charge from the Director, CCDC, 12 Union Road, Cambridge CB2 1EZ, UK (fax: +44-1223-336033; e-mail: deposit@ccdc.cam.ac.uk or http://www.ccdc.cam.ac.uk).

Acknowledgements This study was financially supported by Sinop University in Turkey (Project No. SÜB-1901.14-01) and Hitit University Scientific Research Unit (Project No: FEF19004.15.005). The authors acknowledge Scientific and Technological Research Application and Research Center, Sinop University, Turkey, for the use of the Bruker D8 QUEST diffractometer.

References

1. Hattori M, Hada S, Watahiki A, Ihara H, Shu YZ, Kakiuchi N, Mizuno T, Namba T. Studies on dental caries prevention by traditional medicines. X. Antibacterial action of phenolic components from mace against *Streptococcus mutans*. Chem Pharm Bull. 1986;34(9):3885–93.
2. Erber S, Ringshandl R, von Angerer E. 2-Phenylbenzo[b]furans: relationship between structure, estrogen receptor affinity and cytostatic activity against mammary tumor cells. Anticancer Drug Des. 1991;6(5):417–26.

3. Cui B, Chai H, Reutrakul V, Farnsworth NR, Cordell GA, Pezzutto JM, Kinghorn AD. Novel cytotoxic 1H-cyclopenta[β]benzofuran lignans from *Aglaia elliptica*. Tetrahedron. 1997;53:17625–32.
4. Lee SK, Cui B, Mehta RR, Kinghorn AD, Pezzutto JM. Cytostatic mechanism and antitumor potential of novel 1H-cyclopenta[b]benzofuran lignans isolated from *Aglaia elliptica*. Chem Biol Interact. 1998;115(3):215–28.
5. Kodama I, Kamiya K, Toyama J. Amiodarone: ionic and cellular mechanisms of action of the most promising class III agent. Am J Cardiol. 1999;84(9A):20R–8R.
6. Hayakawa I, Shioya R, Agatsuma T, Furukawa H, Naruto S, Sugano Y. 4-Hydroxy-3-methyl-6-phenylbenzofuran-2-carboxylic acid ethyl ester derivatives as potent anti-tumor agents. Bioorg Med Chem Lett. 2004;14(2):455–8.
7. Hwang BY, Su BN, Chai H, Mi Q, Kardono LB, Afriastini JJ, Riswan S, Santarsiero BD, Mesecar AD, Wild R, Fairchild CR, Vite GD, Rose WC, Farnsworth NR, Cordell GA, Pezzutto JM, Swanson SM, Kinghorn AD. Silvestrol and episilvestrol, potential anticancer rocaglate derivatives from *Aglaia silvestris*. J Org Chem. 2004;69(10):3350–8.
8. Masche UP, Rentsch KM, von Felten A, Meier PJ, Fattinger KE. No clinically relevant effect of Iornoxicam intake on acenocoumarol pharmacokinetics and pharmacodynamics. Eur J Clin Pharmacol. 1999;54(11):865–8.
9. Karaliota A, Kretsi O, Tzougraki C. Synthesis and characterization of a binuclear coumarin-3-carboxylate copper(II) complex. J Inorg Biochem. 2001;84(1–2):33–7.
10. Berk N. Synthesis of benzofuran derivative dithiocarbamate esters. MSc thesis, Adıyaman University; 2013.
11. Kleiner HE, Vulimiri SV, Miller L, Johnson WH, Whitman CP, DiGiovanni J. Oral administration of naturally occurring coumarins leads to altered phase I and II enzyme activities and reduced DNA adduct formation by polycyclic aromatic hydrocarbons in various tissues of SENCAR mice. Carcinogenesis. 2001;22(1):73–82.
12. Tanew A, Ortel B, Rappersberger K, Honigsmann H. 5-Methoxypsoralen (Bergapten) for photochemotherapy. Bioavailability, phototoxicity, and clinical efficacy in psoriasis of a new drug preparation. J Am Acad Dermatol. 1988;18(2):333–8.
13. Gill J, Heel RC, Fitton A. Amiodarone. An overview of its pharmacological properties, and review of its therapeutic use in cardiac arrhythmias. Drugs. 1992;43(1):69–110.
14. Köse DA, Öztürk B, Şahin O, Büyükgüngör O. Mixed ligand complexes of coumarilic acid/nicotinamide with transition metal complexes: synthesis and structural investigation. J Therm Anal Calorim. 2014;115(2):1515–24.
15. Dağlı Ö, Köse DA, Şahin O, Şahin ZS. The synthesis and structural characterization of transition metal coordination complexes of coumarilic acid. J Therm Anal Calorim. 2017;128(3):1373–83.
16. Mirochnik AG, Bukvetskii BV, Zhikhareva PA, Karasev VE. Crystal structure and luminescence of the [Eu(Phen)(2)(NO3)(3)] complex. The role of the ion-coactivator. Russ J Coord Chem. 2001;27(6):443–8.
17. de Farias RF, Airoldi C. Some structural features of MoO3-1,10-phenanthroline intercalation compounds. J Phys Chem Solids. 2003;64(11):2199–204.
18. Leontie L, Druta I, Danac R, Rusu GI. On the electronic transport properties of pyrrolo[1,2-a][1, 10]phenanthroline derivatives in thin films. Synth Met. 2005;155(1):138–45.
19. Mudasir N, Inoue H. Iron(II) and nickel(II) mixed-ligand complexes containing 1,10-phenanthroline and 4,7-diphenyl-1,10-phenanthroline. Transit Met Chem. 1999;24(2):210–7.
20. Nakamoto K. Infrared and Raman spectra of inorganic and coordination compounds. Toronto: Wiley; 1997.
21. Köse DA, Gökçe G, Gökçe S, Uzun İ. Bis(N,N-diethylnicotinamide) p-chlorobenzoate complexes of Ni(II), Zn(II) and Cd(II). J Therm Anal Calorim. 2009;95(1):247–51.
22. Sheldrick GM. A short history of SHELX. Acta Cryst. 2008;A64(1):112–22.
23. Farrugia LJ. WinGX suite for small-molecule single-crystal crystallography. J Appl Cryst. 1999;32:837–8.
24. Mercury. version 3.0; CCDC. www.viaccdc.cam.ac.uk/products/mercury.
25. Spek AL. PLATON—a multipurpose crystallographic tool. Utrecht: Utrecht University; 2005.
26. Köse DA, Şahin O, Büyükgüngör O. Synthesis, spectral, thermal, magnetic and structural study of diaquabis(m-hydroxybenzoato-κO)bis(N,N-diethylnicotinamide-κN)cobalt(II). Eur Chem Bull. 2012;1(6):196–201.
27. Köse DA, Ay AN, Şahin O, Büyükgüngör O. A mononuclear, mixed (salicylato) (nicotinamide) complex of Zn(II) with penta- and hexa-coordination sites: a novel framework structure. J Iran Chem Soc. 2012;9(4):591–7.
28. Köse DA, Necefoğlu H, Şahin O, Büyükgüngör O. Synthesis, structural, spectroscopic characterization, and structural comparison of 3-hydroxybenzoate and nicotinamide/N,N-diethylnicotinamide mixed ligand complexes with Zn(II). J Therm Anal Calorim. 2012;110(3):1233–41.